Soft Matter

Effect of Polyampholyte Net Charge on Complex Coacervation between Polyampholytes and Inorganic Polyoxometalate Giant Anions

Journal:	*Soft Matter*
Manuscript ID	SM-ART-08-2020-001565.R1
Article Type:	Paper
Date Submitted by the Author:	29-Sep-2020
Complete List of Authors:	Ferreira, Manuela; Wayne State University Jing, Benxin; Wayne State University, Lorenzana, Adrian; Wayne State University Zhu, Yingxi; Wayne State University, Department of Chemical Engineering and Materials Science

Effect of Polyampholyte Net Charge on Complex Coacervation between Polyampholytes and Inorganic Polyoxometalate Giant Anions

Manuela Ferreira,[#] Benxin Jing,[#] Adrian Lorenzana, and Yingxi Zhu[*]
Department of Chemical Engineering and Materials Science
Wayne State University, Detroit, MI 48202

Abstract

The effect of net charge of zwitterionic polymers on the phase behavior and viscoelastic properties of hybrid polyampholyte-polyoxometalate (POM) complexes in salted aqueous solutions is investigated with polyampholyte copolymers consisting of both positively and negatively charged monomers. Zwitterionic polyampholytes of varied net charge, abbreviated as PA_xM_y, are synthesized by varying the feeding molar ratio of negatively charged 2-acrylamido-2-methyl-1-propanesulfonic acid (AMPS) to positively charged [3-(methacryloylamino) propyl]trimethylammonium chloride (MAPTAC) monomers in aqueous solution. The coacervate formation between PA_xM_y and inorganic anionic POM, $\{W_{12}\}$ in LiCl added aqueous solutions can be enhanced by increasing the molar fraction of positively charged MAPTAC monomer and LiCl concentration. The salt-broadened coacervation, clearly distinct from the salt-suppressed one between oppositely charged polyelectrolytes, suggests the account of zwitterion-anion pairing for PA_xM_y-$\{W_{12}\}$ coacervate formation due to stronger binding of multivalent $\{W_{12}\}$ giant ions with PA_xM_y than simple ions. Importantly, as AMPS or MAPTAC monomer fraction in polyampholytes is varied by merely ±5% from the effective net neutral case, the viscoelasticity of PA_xM_y-$\{W_{12}\}$ coacervates can be modified by 4-5 folds, suggesting a new tuning parameter to fine control the macroionic interactions and material properties of biomimetic complex coacervates.

[#] M. F. and B.J. equally contributed to this work

[*]Corresponding author (yzhu3@wayne.edu)

Introduction

Macroionic complexation in aqueous solutions between different charged macromolecules, such as colloids, polyelectrolytes, surfactants, and nanoparticles, has received much scientific attention in the past due to their broad applications from nanomedicines to sensor devices[1-4]. Particular interest has recently emerged with spontaneous liquid-liquid phase separating complex coacervation between oppositely charged macromolecules in aqueous media, resulting in a polymer-rich dense coacervate phase and a dilute supernatant phase[5]. Biphasic coacervate complexes have been long studied in biochemical science with their relevance to membraneless organelles[6] and employed in food, pharmaceutical, and cosmetic products for decades[7-10]. Until recently, great interest in synthetic complex coacervates with controllable and desired material properties has arisen to develop new functional materials[11, 12] for drug delivery, underwater adhesion[13-15], and ultrafiltration[16-18]. Hence, it remains critical to understand and control the coacervation between macroions in aqueous media and resulting material properties of macroion coacervates for new material design paradigms.

Essentially, both phase behaviors and material properties of macroionic coacervating materials are underlined by associative binding between charged ionic groups on constituent macroions. For common polyelectrolyte coacervates, the release of counterions near polyelectrolytes upon cation-anion pairing has been arguably accounted for the entropy-driven coacervate formation between oppositely charged polyelectrolytes in aqueous media[19, 20]. Increasing or decreasing charge density of the constituent polyelectrolytes could broaden or narrow the biphasic coacervate phases, respectively [21-24]. It is observed that a critical charge density is present for polyelectrolyte coacervation to occur [25-27]; conversely, if the charge density is too high, solid precipitation rather than biphasic liquid coacervation would occur [28-30]. The associative charging and resulting electrostatic interaction between oppositely charged macroions can be also effectively tuned by their charge density, which could further modify the inter-chain binding relaxation dynamics and viscoelastic properties of macroionic complex coacervates[22, 31, 32]. Traditional weak polyelectrolytes, whose charge density can be tuned by solution pH and added salts, have been investigated as a “smart” building component to develop multi-responsive coacervates and other functional polyelectrolyte complexes with tunable viscoelasticity[33-35]. Previous rheological work has demonstrated that decreasing charge density of polyelectrolytes not only narrows the coacervate phase but also lower shear moduli with faster

relaxation dynamics of polyelectrolytes[21, 24, 36-38]. Furthermore, it has been reported that the blockiness and relative position of charge sequences in polyelectrolytes could also strongly affect polyelectrolyte coacervation. [21, 39, 40] Increasing charge blockiness of such polyelectrolytes can even enhance the salt resistance of their complex coacervates[21, 39].

To date, most research on synthetic macroion coacervates has focused on polyelectrolyte bearing one type of repeated and symmetric charged groups, i.e. simple polycations and polyanions. Conversely, many biological coacervates involve zwitterionic proteins and lipid molecules. In comparison to simple polycations and polyanions, the molecular structures of zwitterionic proteins and synthetic polymers are much more complicated in that a single zwitterionic polymer could carry three types of charge sequences simultaneously: net positive, net neutral, and net negative, which could greatly alter their interaction with themselves and with other polyelectrolytes. Many zwitterionic polymers could form self-coacervate by themselves[41], possibly resulting from the strong interaction between their own charge sequences. One type of the most intriguing biological coacervates, membraneless organelles, consist of zwitterionic intrinsically-disorder proteins (IDPs) whose charge sequence is argued to be responsible for the formation of compartmentalized functional self-coacervate droplets in cells to participant in biological functions[42-45]. Recent theoretical models have captured the effects of charge sequence on the self-coacervation of polyampholytic IDPs with the same net charge, enlightening the complexity that comes from the oppositely charged monomers interactions[45, 46]. Moreover, it is found that the charge sequence of polypeptides as analogues to IDPs is critical to control the phase separation and coacervate stability in a similar fashion to IDP coacervation in nature[41-46]. For specific coacervation cases involving zwitterionic polymers, self-coacervation of polyzwitterions could further complicate the phase behaviors of polyzwitterion-polyelectrolyte coacervation. Therefore, understanding the role of polyzwitterionic net charge on their coacervation with polyelectrolytes is critical to the fundamental science of coacervating materials as well as fine-tuning their material properties.

In our previous work, we have found that dipolar zwitterionic polysulfobetaines with zero net charge could form complex coacervate with anionic inorganic polyoxometalates (POMs) in salted aqueous solution[47, 48]. Furthermore, based on the composition analysis and isothermal titration calorimetric measurements, we have confirmed that the enthalpy change upon polysulfobetaine-$\{W_{12}\}$ coacervation is negligible; the salt concentration in supernatant is higher

that that in dense coacervate while polymer and POM concentrations in dense coacervate are higher than those in supernatant [47, 48]. Thereby we have demonstrated that such hybrid organic-inorganic coacervates are indeed entropy-driven liquid-liquid separating complexes similar to those biological and synthetic polyelectrolyte coacervates [47, 48]. Yet, it is important to note that the entropy gain results from the release of monovalent anions bound with polysulfobetaines and replaced by multivalent anionic POMs to form polyzwitterion-POM associative pairs, which is different from the release of counterions for polyelectrolytes coacervates. POMs are multivalent anionic metal-oxide nanoclusters of 0.8-6 nm in diameter consisting of $\{MO_n\}$ polyhedra[49], where n =4−7 and M is generally Mo, W, V, U, and Nb with well-defined crystalline structure and charge distribution in aqueous solution. With the successful introduction of inorganic POMs, we can significantly enhance the mechanical stability of polysulfobetaine-based coacervates by orders of magnitude[47, 48]. Furthermore, as POMs have been explored as novel functional nanomaterials used for catalysis[50, 51], semiconductors[52], anti-cancer/virus and anti-amyloid treatments[53, 54], introducing POMs to coacervate materials would greatly broaden the functions and applications. However, as polysulfobetaines are zwitterionic polymers whose monomers bear a zwitterionic group with absolutely net charge neutral, they are not suitable to investigate the effect of charge sequence.

In this work, we adopt polyampholytes of tunable net charges by varying the ratio of anionic to cationic monomers and investigate the effect of net charge of polyampholytes on their coacervation with POMs[55]. Specifically, we select the polyampholyte copolymers consisting of negatively charged 2-acrylamido-2-methyl-1-propanesulfonic acid (AMPS) and positively charged [3-(methacryloylamino)propyl]trimethylammonium chloride (MAPTAC) monomers. By varying the molar ratio of AMPS-to-MAPTAC monomers, we can effectively control the net charge of polyampholyte from net negative to nearly net neutral and net positive in aqueous solution. The POM selected in this work is lithium metatungstate, $Li_6H_2W_{12}O_{40}$ ($\{W_{12}\}$) giant molecule of 0.8 nm in diameter and bearing 8 dissociable negative charges in aqueous solution. Herein, we systematically characterize the coacervate formation and viscoelastic properties of polyampholyte-$\{W_{12}\}$ complexes with varied polyampholyte net charge in aqueous solution of varied concentrations of polyampholyte, $\{W_{12}\}$, and added LiCl salt by fluorescence microscopy and rheology.

Experimental Section

Materials. AMPS, 50 wt% MAPTAC aqueous solution, 2,2′-azobis(2-methylpropionamidine) dihydrochloride (AAPH), fluorescein o-acrylate, lithium chloride (LiCl), potassium chloride (KCl), N-[Tris(hydroxymethyl)methyl]-3-aminopropanesulfonic acid (TAPS), 3-(N-Morpholino)propanesulfonic acid (MOPS), 2-(N-Morpholino)ethanesulfonic acid hydrate (MES), potassium acetate, and sodium hydroxide were all purchased from Sigma Aldrich and used directly. $\{W_{12}\}$ was purchased from LMT Liquid and freeze-dried (Labconco Freezone 4.5 Freeze Dryer) before experiments.

Synthesis of polyampholyte copolymers of varied net charge. Solution radical polymerization was adopted to synthesize the polyampholytes copolymer of varied AMPS-to-MAPTAC molar ratios. The resulting copolymer, poly($(AMPS)_x$-co-$(MAPTAC)_y$), as schematically illustrated in **Figure 1a**, is abbreviated as PA_xM_y, where x:y represents the feeding monomer molar ratio of m_{AMPS}:m_{MAPTAC}. In this work, we mainly focus on three polyampholytes: $PA_{45}M_{55}$, $PA_{50}M_{50}$, and $PA_{55}M_{45}$, corresponding to x:y = 45:55, 50:50, and 55:45, respectively. $PA_{47.5}M_{52.5}$ and $PA_{52.5}M_{47.5}$ corresponding to x:y = 47.5:52.5, and 52.5:47.5 were also synthesized to verify the control and trend of PA_xM_y net charge by varying x:y ratios as reported in this work. It is noted that all the PA_xM_y copolymers were synthesized at the similar solution conditions except their respective x:y feeding ratios.

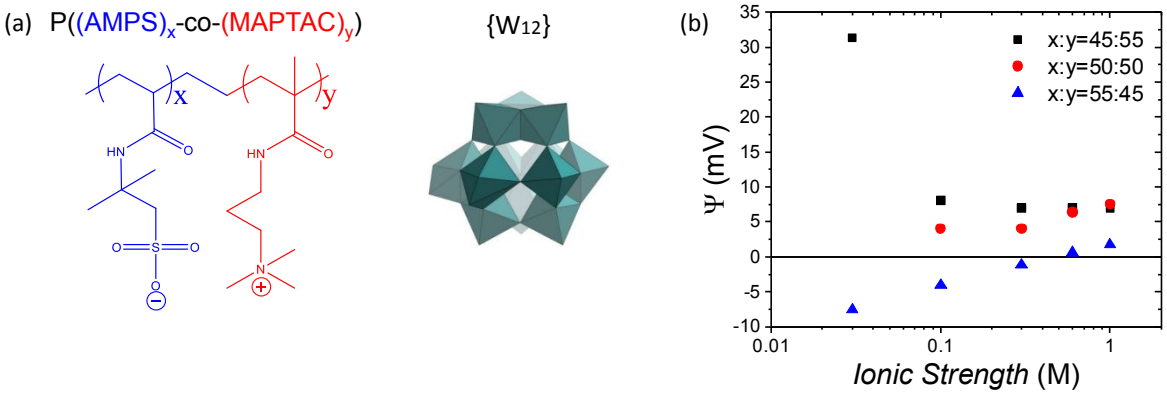

Figure 1. (a) Schematic illustration of chemical structure of polyampholyte P($(AMPS)_x$-co-$(MAPTAC)_y$), PA_xM_y and lithium metatungstate, $\{W_{12}\}$. **(b)** Measured electric potential of $PA_{45}M_{55}$, $PA_{50}M_{50}$, and $PA_{55}M_{45}$ against ionic strength of salt added aqueous solution.

To synthesize $PA_{45}M_{55}$, as an example of PA_xM_y copolymerization procedure, 18.65 g of AMPS was dissolved in 100 mL deionized water (Barnstead Smart2Pure) and neutralized by 3.6 g sodium hydroxide. Subsequently, 48.56 g MAPTAC solution, which contains 50 wt% MAPTAC in deionized water, was added to the AMPS mixture. Deionized water was added to further dissolve the mixture under vigorous stirring, yielding an AMPS and MAPTAC mixed solution of total 350 mL in volume. Sodium bicarbonate was added to the mixture to adjust the solution pH ~ 7.0. After being purged with pure nitrogen gas for 30 minutes, the solution was heated to 78 °C in a nitrogen protected atmosphere under constant stirring at a speed of 350 rpm. Then 0.3 g AAPH dissolved in 5 ml deionized water was added to the solution at an equal interval dose of 1 mL every hour for the first 5 hours, followed by incubation at 78 °C for additional 7 hours. After polymerization, the products were cooled and dialyzed (Spectrum™ Spectra/Por™ regenerated cellulose tubing, 25 kD MWCO) in deionized water for 7 days to remove the salt. After the dialysis, the aqueous solution of polyampholytes was cooled to 4 °C so that they would spontaneously separate into dense and dilute phases as the upper critical solution temperature (UCST) of some polyampholytes in deionized water is higher than room temperature, which is similar to the UCST behavior of other zwitterionic polymers[56-58]. The dense phase of PA_xM_y was collected after centrifugation to remove its supernatant and dried by freeze-drying. Other PA_xM_ys of varied x:y ratios were synthesized by following the same procedure with correspondingly varied amounts of AMPS and MAPTAC with respect to the desired monomer ratios. Fluorescence-labeled PA_xM_y (f-PA_xM_y) polyampholytes was synthesized via copolymerization with 0.5 mol% fluorescein O-acrylate.

To prepare homogeneous polyampholyte aqueous solution at room temperature, LiCl or $\{W_{12}\}$ was added, which can significantly lower the UCST of the polyampholytes to be below 0 ℃ and eliminates the "self-coacervate" phase separation behavior occurred between the polyampholytes themselves [48, 56, 57]. In this system, adding LiCl to PA_xM_y aqueous solutions at LiCl concentration higher than 0.05 M could ensure homogenous PA_xM_y aqueous solution at T > 0 ℃. In this work, we chose LiCl because of its higher solubility in $\{W_{12}\}$ aqueous solution than other commonly used salts such as NaCl and KCl. It is noted that adding LiCl causes no change in the solubility of $\{W_{12}\}$ or any $\{W_{12}\}$ aggregation in aqueous solution when the concentration of LiCl is below 6.0 M, in sharp contrast to much lower solubility of $\{W_{12}\}$ in the aqueous solution added with other common salts such as NaCl and KCl.

Preparation and characterization of polyampholyte-{W_{12}} complexes. PA_xM_y -{W_{12}} complexes were prepared by mixing PA_xM_y/LiCl solution with {W_{12}} solution of varied molar ratio of total {W_{12}} charges (=8 × {W_{12}} molar concentration) to total A_xM_y molar concentration, which was estimated according to the molecular weight, M_w of A_xM_y monomer, $M_w(A_xM_y) = x \times M_w(AMPS)/50 + y \times M_w(MAPTAC)/50$. It should be noted that both PA_xM_y and {W_{12}} solutions were completely homogenous and clear before mixing. Upon mixing, the formation of phase separated coacervates and gel-like complexes was observed immediately by naked eyes. The phase behaviors of PA_xM_y-{W_{12}} complexation was further examined by confocal laser scanning microscopy (CLSM, Carl Zeiss LSM780) with a 63x objective lens (Plan-Apochromat, NA = 1.4, oil immersion) and an Airyscan detector (Carl Zeiss), using fluorescein labeled polyampholyte at the f-PA_xM_y to plain PA_xM_y weight ratio of 1:9 in aqueous solution. All the complex morphology reported in this work was carried out at constant temperature of 22 ℃.

The electric potential of PA_xM_y in aqueous solution with added salt was determined based on the pK_a shift of f-PA_xM_y from that of free fluorescein in aqueous solutions of the same salt concentrations by titration using a UV-Vis spectrophotometer (V-630, JASCO). The experiment was performed in a four-component "Good" buffer solution including 5 mM potassium acetate, MES, MOPS, and TAPS with pK_a = 4.76, 6.1, 7.2, and 8.4, respectively, whose contribution to the ionic strength of PA_xM_y aqueous solution is negligible at varied pH. The solutions pH was tuned using KOH or HCl.

The partition of {W_{12}} and Cl^- anions in dense and supernatant phases of PA_xM_y-{W_{12}} complex coacervates were determined directly by x-ray fluorescence (XRF) spectrometer (Shimadzu, EDX-7000). After separating the supernatant and dense coacervate phases through repeated centrifugation, the weight fraction of tungsten, chlorine, and sulfur elements in each phase is obtained by XRF. LiCl concentration in dense and supernatant phases LiCl concentration in the supernatant and coacervate phase was determined by titrating Cl^- using $AgNO_3$ with K_2CrO_4 as an indicator (aka, the Mohr's Method) [59, 60]. The Mohr's method is known as an extremely sensitive and accurate method to determine chlorine concentration with a relative standard deviation ≤ 0.07%.[61]

The linear and nonlinear viscoelastic properties of PA_xM_y-{W_{12}} dense coacervates were characterized by a stress-controlled rheometer (Malvern, Gemini HR nano) with a parallel plate

fluid cell of 20 mm in diameter and 1000 μm in gap spacing. All the dense coacervate samples were centrifuged at 22,800 g for at least 1 h at T = 22 ℃ to thoroughly remove all the supernatant that could be trapped in the coacervate. To avoid any slip of the samples during shear, the surfaces of parallel plates were glued with sandpaper of grit size 600 (47185A51, McMaster-Carr). After sample loading and reaching the desired gap spacing between the parallel plates, a thin layer of paraffin oil (Sigma-Aldrich) was carefully applied to seal the edge of the sample to prevent solvent evaporation during the experiment. For linear rheology experiments, oscillatory shear measurements at constant strain γ = 1% and varying angular frequency ω = 0.19 - 62.83 rad/s was conducted at a fixed temperature, T that was varied from 2 to 58 ℃, controlled by a Peltier Element. At each temperature, a time period of 10 minutes was waited to ensure thermal equilibrium before data acquisition. For non-linear rheology experiments, oscillatory shear measurements were conducted against increasing γ at constant ω = 2.6 rad/s and T = 22 ^{o}C.

Results and Discussion

With successful synthesis of zwitterionic PA_xM_y copolymers, we first determine their net charge against varied x:y molar ratios in aqueous solution with added salt at a fixed concentration of 0.03 – 1.0 M by electric potential measurements. Given that LiCl used in this work may affect the accuracy of measured pH value due to the confusion of Li^+ with H^+ by a pH meter and the resulting measured pK_a of fluorescein dye[62-64], the electric potential was measured using KCl of the same ionic strength instead of LiCl. We use f-PA_xM_y to determine the pKa shift of polyampholyte-bound fluorescein from that of free fluorescein at the same ionic strength by UV-vis spectroscopy. UV-vis absorbance of f-PA_xM_y is measured at the wavelength of 500 nm, Abs_{500}, which is the strongest and most pH-sensitive absorption peak resulting from the protonation and de-protonation of the phenol group in fluorescein[64], as shown in **Figure S1**. The decrease of Abs_{500} peak value with decreasing pH leads to typical titration curves in order to determine the pKa of PA_xM_y-bound fluorescein, $pK_{a,f-PA_xM_y}$ in comparison to that of free fluorescein, $pK_{a,f}$ in the salt-added solution. The electric potential, Ψ, of PA_xM_y is estimated according to the simplified Boltzmann equation, $\Psi = k_BT(pK_{a,f} - pK_{a,f-PA_xM_y})ln10/e$ [48]. As summarized in **Figure 1b**, we confirm that the net charge of PA_xM_y is indeed varied with x:y molar ratio as well as solution ionic strength. At a given ionic strength particularly at low salt, the net charge of PA_xM_y exhibits a transition from net positive to net negative as increasing x-to-

y molar ratio by merely 5% deviation from the equal monomer ratio. Such a trend is expected with the increase of the fraction of negatively charged sulfonic acid terminal group accompanied with the decrease of positively charged trimethylammonium terminal group in PA_xM_y copolymers. The monotonic change in the net charge with ionic strength could be attributed to combining result of the net amount of K^+ and Cl^- ions bound to PA_xM_y at a given x:y molar ratio and enhanced electrostatic screening effect with increased salt concentration[65-68]. However, it is noted that due to lack of theoretical prediction to directly relate the measured electrical potential to the effective charge density of zwitterionic polymer, in this work we simply designate the polyampholytes as "net positively charged", "net neutral", or "net negatively charged" based on the sign of measured electrical potential at a given salt concentration. Thus, we observe net positively charged $PA_{45}M_{55}$ and nearly net "neutral" or weakly positively charged $PA_{50}M_{50}$ at all varied ionic strength. Conversely, $PA_{55}M_{45}$ shows a transition from net negatively to weakly net positively charged as increasing ionic strength.

Below we then focus on the effect of net charge of PA_xM_y on the complexation between zwitterionic PA_xM_y and anionic $\{W_{12}\}$ in LiCl aqueous solution. The phase behavior of PA_xM_y-$\{W_{12}\}$ complexation is studied against the molar ratio $C_{e^-(W12)}/C_{A_xM_y}$ at constant PA_xM_y monomer concentration, $C_{A_xM_y} =$ 89.6 mM and LiCl concentration, C_{LiCl} = 0.2 M. As the photographs are shown in **Figure 2a-c**, each PA_xM_y polyampholytes of varied x:y ratio exhibit similar phase behaviors upon mixing with $\{W_{12}\}$ in LiCl aqueous solutions, including homogeneous solution, biphasic complex coacervate, monophasic gel or solution as increasing $C_{e^-(W12)}/C_{A_xM_y}$. The transition from biphasic liquid-liquid separating coacervates to monophasic complex gel or solution with increasing $C_{e^-(W12)}/C_{A_xM_y}$ can be clearly observed by naked eyes and further confirmed by fluorescence microscopy. The coacervate-to-gel transition usually occurs with higher initial polyampholyte concentration. We can distinguish the monophasic gel phase from the solution based on the cloudiness, as a gel (see the photographs shown in Figure 1a for $C_{e^-(W12)}/C_{A_{45}M_{55}} = 2000$ % and 1b for $C_{e^-(W12)}/C_{A_{50}M_{50}} = 130$ %) appears cloudy in sharp contrast to a clear solution (see the photograph shown in Figure 1c- for $C_{e^-(W12)}/C_{A_{55}M_{45}}$100%). The coacervate-to-solution transition with net negatively charged $PA_{55}M_{45}$ at the same PA_xM_y concentration with the other two suggests weaker $PA_{55}M_{45}$-$\{W_{12}\}$ association as further discussed on the effect of net charge on the phase diagram of PA_xM_y-

$\{W_{12}\}$ coacervation. It is mostly interesting to find that net negatively charged $PA_{55}M_{45}$ could also form complex coacervates with anionic $\{W_{12}\}$, strongly suggesting that the dominated interaction between PA_xM_y and $\{W_{12}\}$ may not be cation-anion pairing that is accounted for conventional polyelectrolyte complexation[19, 69]. We further check the microstructure of the PA_xM_y-$\{W_{12}\}$ coacervate phase by fluorescence morphological characterization with f-PA_xM_y added to the mixtures as shown in **Figure 2d-f**. For all three PA_xM_y polyampholytes, we observe that fluorescent droplets of dense coacervate corresponding to polyampholyte-rich phase are dispersed in the nearly non-fluorescent solution corresponding to polyampholyte-poor dilute supernatant, similar to those in polysulfobetaine-POM complex coacervates where the dense coacervate phase is both polymer-rich and POM-rich phase [40]. Yet the dense phase of $PA_{45}M_{55}$-$\{W_{12}\}$ coacervates in **Figure 2d** appear to be a biphasic fluid, in sharp contrast to the homogeneous dense phase of $PA_{50}M_{50}$-$\{W_{12}\}$ and $PA_{55}M_{45}$-$\{W_{12}\}$ coacervates as shown in **Figure 2e-f**, respectively. Thus $PA_{45}M_{55}$-$\{W_{12}\}$ complex coacervates appears to be a triphasic coacervating system, whose third phase showing the highest fluorescence seems to be $PA_{45}M_{55}$-$\{W_{12}\}$ aggregates resulting from strong electrostatic interaction between excess cations of $PA_{45}M_{55}$ and anion of $\{W_{12}\}$. Unfortunately, it is currently difficult to further reveal the detailed triphasic structure of $PA_{45}M_{55}$-$\{W_{12}\}$ coacervates due to the unavailability of suitable characterization facility on-site.

In our previous work, we have elucidated the entropy-driven coacervation between zwitterionic polysulfobetaines, which bear zwitterion as the side group of monomers, and anionic $\{W_{12}\}$ via zwitterion-anion pairing upon releasing the simple anions previously bound with polysulfobetaines. To examine whether the PA_xM_y-$\{W_{12}\}$ coacervation undergoes the same mechanism as polysulfobetaine-$\{W_{12}\}$ coacervation, we conduct the composition analysis of $\{W_{12}\}$ and Cl^- in supernatant and coacervate phases by XRF and titration of Cl^- by $AgNO_3$. As the XRF results are shown in **Figure 3a**, the measured weight fractions of both tungsten and sulfur elements in the dried dense coacervates are clearly higher than those in the supernatant while the weight fraction of chlorine element in the supernatant is higher than that in the dense coacervate. Thus, for all the PA_xM_y of varied net charge, the dense coacervate is indeed PA_xM_y- and $\{W_{12}\}$-rich phase while the supernatant is the LiCl-rich phase, consistent with previously reported compositions in biphasic polysulfobetaine-$\{W_{12}\}$ coacervates. The composition analysis strongly suggests entropy-driven thermodynamic process for PA_xM_y-$\{W_{12}\}$ coacervation.

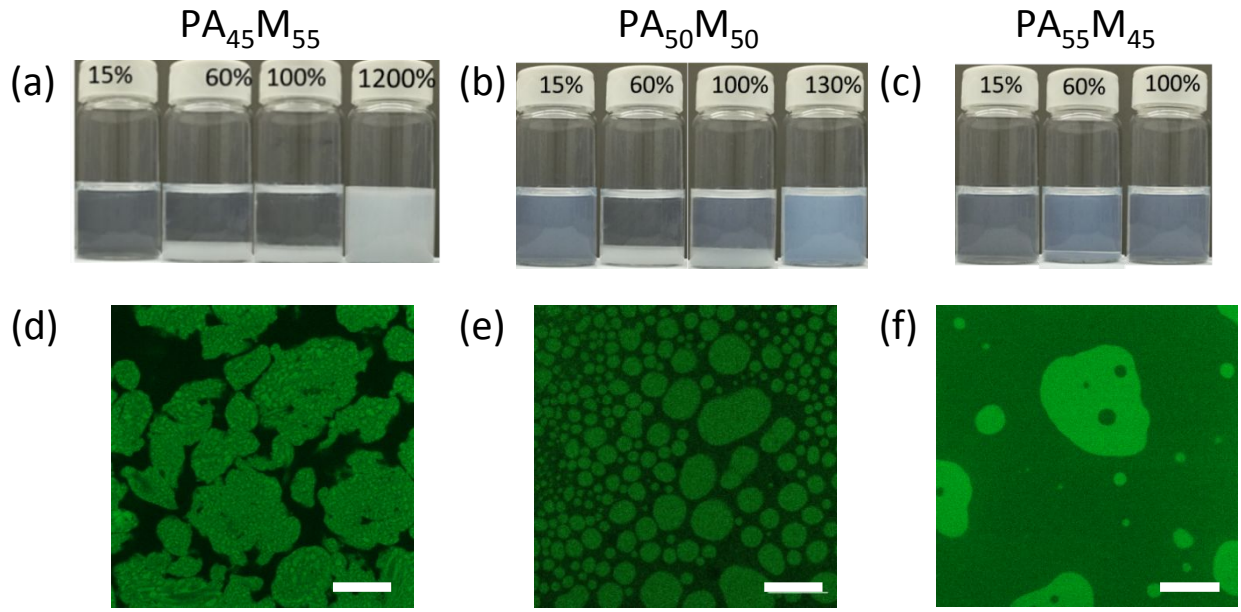

Figure 2. (Two-column Figure) Digital photographs of PA_xM_y-$\{W_{12}\}$ complexes formed against increased $C_{e^-(W12)}/C_{A_xM_y}$ in the range 15-1200% at constant $C_{A_xM_y}$= 89.6 mM and C_{LiCl} = 0.2 M correspond to the cases of **(a)** $PA_{45}M_{55}$, **(b)** $PA_{50}M_{50}$, and **(c)** $PA_{55}M_{45}$. Representative microscopic morphological structures of biphasic liquid-liquid separating PA_xM_y-$\{W_{12}\}$ coacervates formed at $C_{A_xM_y}$= 89.6 mM, $C_{e^-(W12)}/C_{A_xM_y}$= 60%, and C_{LiCl}= 0.2 M correspond to the cases of **(d)** $PA_{45}M_{55}$, **(e)** $PA_{50}M_{50}$, and **(f)** $PA_{55}M_{45}$. All the fluorescence micrographs were acquired by CLSM with corresponding f-PA_xM_y added to polyampholyte aqueous solutions immediately after mixing with $\{W_{12}\}$ solutions. The scale bar shown in **(d)-(f)** is 20 μm.

It is also observed that at a given initial salt concentration, the difference of LiCl concentrations between the dense and supernatant phases first increases and then decreases with increasing $C_{e^-(W12)}/C_{A_xM_y}$ as a representative case of $PA_{50}M_{50}$-$\{W_{12}\}$ coacervates is shown in **Figure 3b**. The observed non-monotonic trend of LiCl partition in dense and supernatant phases also suggests that LiCl indirectly participates in the associative binding between PA_xM_y and $\{W_{12}\}$ and could strongly affects the phase behaviors of PA_xM_y-$\{W_{12}\}$ complexation. Specifically, we speculate that the non-monotonic salt concentration in the dense coacervate against $C_{e^-(W12)}/C_{A_xM_y}$ may result from varied associative interaction between PA_xM_y and $\{W_{12}\}$ for their coacervation, which is also manifested in the viscoelastic behaviors of dense coacervates. Firstly, it is noted that multivalent $\{W_{12}\}$ could work as a crosslinker with PA_xM_y and/or as a macroion to modify the net charge and conformation of PA_xM_y in aqueous solution. At low $\{W_{12}\}$ concentration, the crosslinking effect could dominate and lead to PA_xM_y -$\{W_{12}\}$

association. In this concentration ration regime, a very small number of Cl^- ions are replaced by $\{W_{12}\}$ for the onset of coacervation and its concentrations in the two phases approximate to each other within experimental uncertainty. As increasing $\{W_{12}\}$ concentration, more PA_xM_y -$\{W_{12}\}$ association leads to the release of increased number of Cl^- ions to the supernatant. However, as further increasing $\{W_{12}\}$ concentration, increased electrostatic repulsion between PA_xM_y -bound $\{W_{12}\}$ macroions could result in more swollen PA_xM_y chains and thereby allow more Cl^- to stay near polyampholyte chains. $C_{e^-(W12)}/C_{A_xM_y}$-dependent microstructures of PA_xM_y-$\{W_{12}\}$ dense coacervates is supported by distinct viscoelastic behaviors of dense coacervates as discussed below (See Figure 5 and Supporting Figure S5 and S6). Yet further understanding of the non-monotonic behavior of salt partition in PA_xM_y-$\{W_{12}\}$ coacervates could warrant future study.

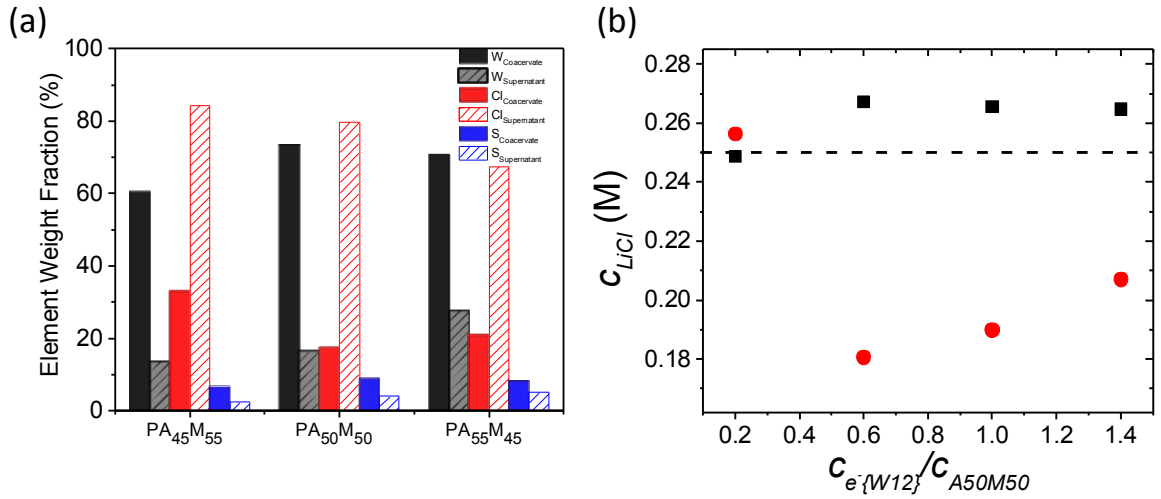

Figure 3. (a) Measured weight fraction of tungsten (black column), chlorine (red column), and sulfur (blue column) element in dense coacervate (solid filled column) and supernatant (shaded column) phase of PA_xM_y-$\{W_{12}\}$ coacervates formed at fixed $C_{A_xM_y}$ = 89.6 mM, $C_{e^-(W12)}/C_{A_xM_y}$ = 60%, and C_{LiCl} = 0.6 M by XRF. **(b)** Measured LiCl concentration in dense coacervate (red circles) and supernatant (black squares) of $PA_{50}M_{50}$-$\{W_{12}\}$ coacervates formed at fixed $C_{A_{50}M_{50}}$ = 89.6 mM, $C_{e^-(W12)}/C_{A_{50}M_{50}}$ = 60%, and C_{LiCl} = 0.25 M. Dash line indicates the initial salt concentration in aqueous solution.

$C_{e^-(W12)}/C_{A_xM_y}$-C_{LiCl} phase diagrams for PA_xM_y-$\{W_{12}\}$ coacervate formation with contrasting net positively charged $PA_{45}M_{55}$ and net negatively charged $PA_{55}M_{45}$ are exhibited in **Figure 4a-b**, respectively. In comparison between the cases of $PA_{45}M_{55}$ and $PA_{55}M_{45}$, we observe that the lower critical $C_{e^-(W12)}/C_{A_xM_y}$ for the solution-to-coacervate transition keeps

nearly constant while the upper critical $C_{e^-(W12)}/C_{A_xM_y}$ for coacervate-to-gel transition as well as gel-to-solution transition decreases with increasing x:y ratio. A clear shift in the upper critical $C_{e^-(W12)}/C_{A_xM_y}$ concentrations for PA_xM_y-$\{W_{12}\}$ coacervate formation at fixed $C_{A_xM_y} =$ 89.6 mM and C_{LiCl} = 0.2 M is observed with varied x:y ratio as shown in **Figure 4c**. It appears that the upper critical $C_{e^-(W12)}/C_{A_xM_y}$decreases with increasing the fraction of negatively charged AMPS blocks in the polyampholyte. The gel phase could disappear for $PA_{55}M_{45}$-$\{W_{12}\}$ complexation at the same $C_{A_xM_y}$. Alternatively speaking, as the net charge of PA_xM_y varies from being net positive to net negative, PA_xM_y-$\{W_{12}\}$ coacervate regime is narrowed, suggesting that net positive polyampholytes could be more favored to form coacervates with anionic $\{W_{12}\}$ than net neutral or net negative ones. However, we observe that for both $PA_{45}M_{55}$ and $PA_{55}M_{45}$, increasing LiCl concentration could significantly broaden the coacervate regime with the shift of the upper critical $C_{cr,\ e^-(W12)}/C_{A_xM_y}$ to higher values, above which the biphasic coacervates will turn to monophasic gel or solution. Clearly, such a trend is distinct with salt-induced suppression of conventional polyelectrolytes coacervation, where increasing salt concentration narrows the coacervate phase due to the electrostatic screening effect. Therefore, it suggests that the binding between PA_xM_y and $\{W_{12}\}$ cannot be regarded as simple cation-anion pairing or between positively charged MAPTAC monomer and $\{W_{12}\}$. Conversely, such salt dependence is consistent with our previous report of salt-broadened coacervation between polysulfobetaines and $\{W_{12}\}$ in salted water[48]. We attribute the salt-broadened coacervation to the "anti-polyelectrolyte" behavior of zwitterionic polymers in aqueous solution[48]. In this work, added LiCl or $\{W_{12}\}$ can bind with PA_xM_y to disrupt the interaction between their cationic and anionic monomers, leading to lower the upper critical solution temperature of PA_xM_y in aqueous solution and higher solubility and charge density in aqueous media. Nevertheless, the salt-poor coacervate phase and the salt-enhanced coacervation as combined suggest that the association between PA_xM_y and $\{W_{12}\}$ also results from zwitterion-anion pairing similar to polysulfobetaines-$\{W_{12}\}$ coacervate. Thereby it supports a general picture that entropy-driven coacervation could occur between polyanions and polyzwitterions, the latter of which includes polypeptides, proteins, and a large selection of biocompatible protein-analogous polymers.

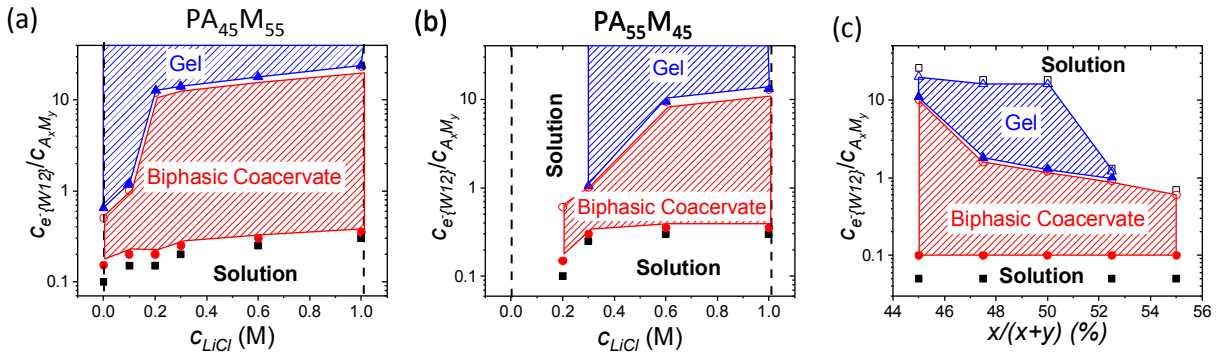

Figure 4. (Two-column Figure) The effect of LiCl concentration on the phase diagram of PA_xM_y $-\{W_{12}\}$ complex formation at constant PA_xM_y monomer concentration, $C_{A_xM_y} =$ 89.6 mM for **(a)** $PA_{45}M_{55}$ and **(b)** $PA_{55}M_{45}$. The lower (red circles) and upper (blue triangles) critical $C_{e^-(W12)}/C_{A_xM_y}$ for coacervate formation are determined by CLSM, where the transitions from monophasic solution to biphasic coacervate and from biphasic coacervate to monophasic gel are observed, respectively. The vertical dash lines shown in panel (a) and (b) indicate the range of C_{LiCl} varied from 0-1.0 M in this work. **(c)** The effect of x:y molar ratio of PA_xM_y in terms of AMPS (x) monomer fraction on the phase diagram of PA_xM_y – $\{W_{12}\}$ complex formation at constant $C_{A_xM_y}$= 89.6 mM and C_{LiCl}= 0.2 M. For all diagrams, three distinct phases, including homogeneous solution (black squares), biphasic liquid-liquid coacervate complex (red circles), and monophasic gel complexes (blue triangles) are observed by CLSM.

Next, we raise the question of how the net charge or charge sequence of polyampholytes could modify the phase behavior and materials properties of PA_xM_y-$\{W_{12}\}$ coacervates. It has been reported that PA_xM_y-based polyampholytes contain three types of monomer sequences: negative -A-A-A, positive -M-M-M-, and net neutral -A-M-A-M-, while more than 60% -A- and -M- monomers are found in the alternating sequence of -A-M-A-M- when x:y is close to 50:50 [70]. Therefore, PA_xM_y synthesized in this work can be pictured as a polymer that displays long neutral zwitterionic sequence doped with some short-charged sequences. As we vary the x:y molar ratio slightly away from being 50:50, the short charged sequences of PA_xM_y are effectively modified, leading to the shift to net negatively charged and net positively charged for $PA_{45}M_{55}$ and $PA_{55}M_{45}$, respectively, in comparison to nearly net neutral $PA_{50}M_{50}$. **Figure 1b** indicates that the charged sequences become mostly screened when ionic strength is greater than 0.1 M, above which PA_xM_y-$\{W_{12}\}$ coacervation is mostly observed. It thereby suggests the account of zwitterion-anion interaction for PA_xM_y-$\{W_{12}\}$ coacervation.

The results above also suggest the effect of net charge on the binding strength between polyampholyte and $\{W_{12}\}$ in their complex coacervates, possibly following the trend of $PA_{45}M_{55}$

> $PA_{50}M_{50}$ > $PA_{55}M_{45}$. The trend of PA_xM_y-{W_{12}} binding strength is first supported by the observed increase of the cloudiness of dense PA_xM_y-{W_{12}} coacervates. As the photographs of glass vials at the same $C_{e^-(W12)}/C_{A_xM_y}$ = 60-100% are shown in **Figure 2a-c**, the coacervate formed with net positively charged $PA_{45}M_{55}$ appears the most cloudy while the one formed with net negatively charged $PA_{55}M_{45}$ appears nearly transparent and the least cloudy. To quantitatively examine it, we carry out frequency-sweep oscillatory shear experiments with dense coacervates formed with $PA_{45}M_{55}$, $PA_{50}M_{50}$, and $PA_{55}M_{45}$ at fixed $C_{A_xM_y}$ = 89.6 mM, $C_{e^-(W12)}/C_{A_xM_y}$ = 60%, and C_{LiCl} = 0.2 M but varied T. To enable reliable and reproducible rheological characterization, we ensure that dense coacervates are free of supernatant phase, which is confirmed by the morphology free of mobile and coalescent liquid droplets with corresponding f-PA_xM_y added in dense coacervates by super-resolution fluorescence microscopy as shown in Supporting **Figure S2**. We observe strong thermo-responsive behavior in the frequency-sweep linear viscoelasticity of PA_xM_y−{W_{12}} dense coacervates at varied T = 2 - 58 ^oC (see Supporting **Figure S3)**. Temperature-dependent viscoelasticity of PA_xM_y−{W_{12}} coacervates could be attributed to weakened zwitterion-anion interaction at higher temperature because it is essentially dipole-dipole interaction[71]. We have performed the standard analysis of time−temperature superposition to rescale all the linear frequency-dependent shear spectra (see Supporting **Figure S4** for T-dependent shifting factors, a_T) and obtain the master curves for PA_xM_y−{W_{12}} dense coacervates as shown in **Figure 5a**. It is observed in **Figure 5a** and Supporting **Figure S3** that at low rescaled angular frequency, ωa_T, the measured loss moduli, G″ is predominately larger than the storage moduli, G′, suggesting liquid-like behavior of dense coacervates. It is more interesting to observe that over a considerably large range of ωa_T spanning nearly 3-5 orders of magnitude, G′ and G″ of all the dense coacervates overlap and both nearly scale with $\omega^{\sim 0.35}$, strongly suggesting a critical-gel-like dynamic structure as we previously observed with polysulfobetaine-{W_{12}} coacervates [47, 72, 73]. In contrast, at higher $C_{e^-(W12)}/C_{A_xM_y}$, we observe simple viscoelastic behavior of monophasic PA_xM_y−{W_{12}} gels: a terminal relaxation time can be well determined as the reciprocal of the ω at which the crossover of G′ and G″ is observed in Supporting **Figure S5 and S6**. Distinct viscoelastic behavior against $C_{e^-(W12)}/C_{A_xM_y}$ for varied PA_xM_y−{W_{12}} complexes in Supporting **Figure S6** agree well with the observed coacervate-to-gel transition as shown in **Figure 2**.

We also examine the non-linear viscoelastic behavior of PA_xM_y–-$\{W_{12}\}$ dense coacervates at fixed ω = 6.28 rad/s, $C_{e^-(W12)}/C_{A_xM_y}$= 60% and C_{LiCl}= 0.2 M and T = 22 °C against shear strain amplitude, γ is shown in **Figure 5b**. When γ is below a critical shear strain, γ_c, both G' and G'' of dense coacervates are nearly constant against γ. It is also noted that for $PA_{45}M_{55}$ and $PA_{50}M_{50}$, G' and G'' nearly overlap at $\gamma<\gamma_c$, confirming the critical gel structure at low shear. As increasing shear deformation amplitude, we observe the typical shear-thinning behavior for all the three dense coacervates: G'' exceeds G' at $\gamma>\gamma_c$, suggesting the rupture of gel-like network in the coacervates [72, 73].

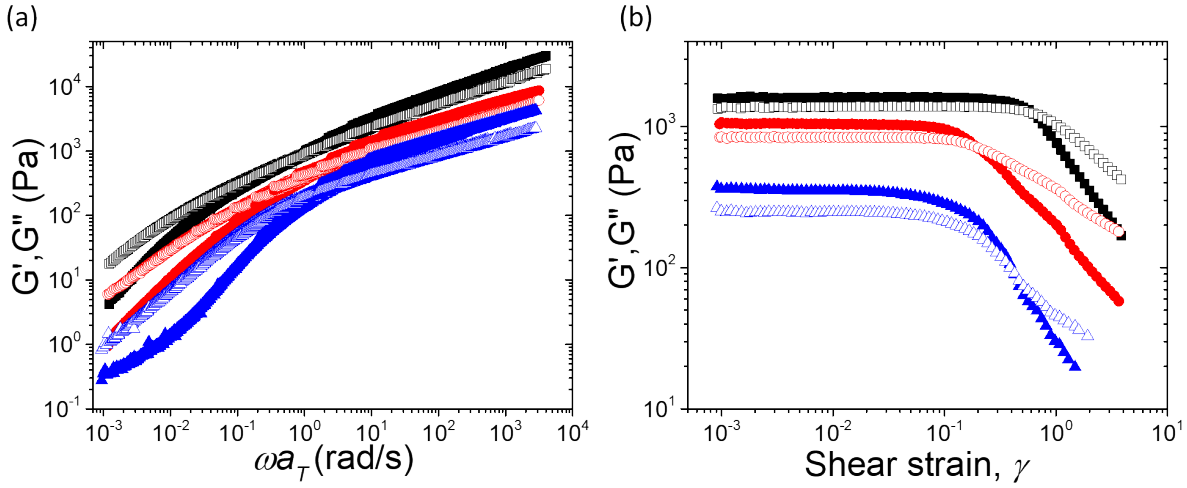

Figure 5. (a) Temperature-frequency superposition master curves of linear shear viscoelastic spectra for $PA_{45}M_{55}$–$\{W_{12}\}$ (black squares), $PA_{50}M_{50}$ –$\{W_{12}\}$ (red circles), and $PA_{55}M_{45}$ –$\{W_{12}\}$ (blue triangles) dense coacervates. Elastic moduli, G' (solid symbols) and viscous moduli, G'' (open symbols) are plotted against shifted angular frequency, ωa_T at constant γ=1%. **b)** γ-dependent viscoelastic spectra of PA_xM_y – $\{W_{12}\}$ dense coacervates formed at constant $C_{A_xM_y}$ = 89.6 mM, $C_{e^-(W12)}/C_{A_xM_y}$= 60%, and C_{LiCl}= 0.2 M with $PA_{45}M_{55}$ (black squares), $PA_{50}M_{50}$ (red circles), and $PA_{55}M_{45}$ (blue triangles) at constant T = 22°C.

Importantly, we discover that despite similar linear and non-linear viscoelastic behaviors among three PA_xM_ys of varied x:y molar ratios, both the strength of measured shear moduli and γ_c follow the same trend of $PA_{45}M_{55}$ > $PA_{50}M_{50}$ > $PA_{55}M_{45}$ as summarized in **Figure 6a-b**, respectively**.** Both results clearly suggest the stronger interaction of $\{W_{12}\}$ with net positively charged $PA_{45}M_{55}$ than nearly net neutral $PA_{50}M_{50}$ and net negatively charged $PA_{55}M_{45}$ upon their complex coacervation. It is also important to note that by varying either AMPS or MAPTAC monomer fraction by merely ±5% from the effective net neutral case, the shear moduli could be

effectively modify by 4-5 times while γ_c could be shifted nearly one order of magnitude between ~ 10% and ~ 70%. Hence, it suggests that the net charge of zwitterionic polymers could be a simple tuning parameter in designing polyions to fine control the interaction and material properties of complex coacervates without altering their phase behaviors as concentrations or environmental variables do conversely.

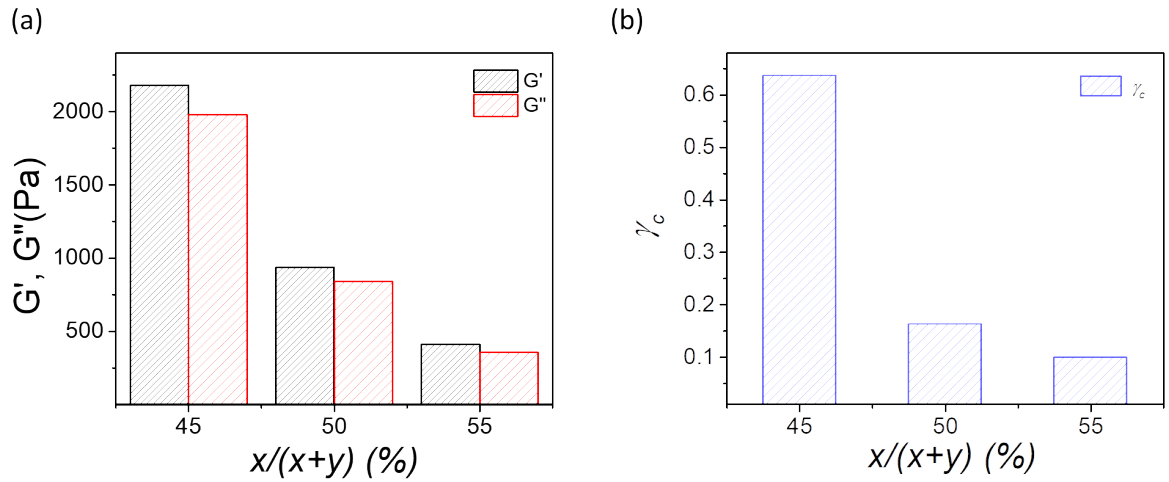

Figure 6. Comparison of **(a)** measured elastic moduli, G' (filled column) and viscous moduli, G'' (shaded column) at 1 Hz and room and **(b)** critical strain, γ_c where linear to non-linear shear behavior is observed in Figure 4b, of PA_xM_y-$\{W_{12}\}$ dense coacervates against AMPS (x) monomer fraction. All the coacervates are of formed at constant $C_{A_xM_y}$ = 89.6 mM, $C_{e^-(W12)}/C_{A_xM_y}$= 60%, and C_{LiCl}= 0.2 M and at temperature.

Conclusion

In summary, we have successfully demonstrated the generality of macroion coacervate formation between zwitterionic polyampholyte copolymers of varied net charges and inorganic POM anions in salted aqueous solutions. By varying the respective x:y molar ratio of negatively charged AMPS to positively charged MAPTAC monomer, we have effectively control the net charge of PA_xM_y polyampholyte copolymers from net negative ($PA_{55}M_{45}$) to nearly net neutral ($PA_{50}M_{50}$) to net positive ($PA_{45}M_{55}$) in salted aqueous solution. Thereby we have examined the effect of net charge of PA_xM_y on the phase diagram and viscoelastic properties of PA_xM_y-$\{W_{12}\}$ coacervates in LiCl aqueous solution. As increasing the concentration ratio of $\{W_{12}\}$ to PA_xM_y, we have observed the transition from homogeneous solution to liquid-liquid phase separated

coacervate and then to monophasic gel in PA_xM_y-$\{W_{12}\}$ mixtures. Similar to the previously reported entropy-driven coacervation between zwitterionic polysulfobetaine homopolymers and anionic $\{W_{12}\}$, we have further confirmed that PA_xM_y-$\{W_{12}\}$ coacervate phase becomes broadened with increasing LiCl concentration in aqueous solution due to the competitive binding of multivalent $\{W_{12}\}$ with PA_xM_y against monovalent Cl^-. Such salt-broadened phase suggests that zwitterion-anion pairing is responsible for PA_xM_y-$\{W_{12}\}$ coacervation, distinct from cation-anion pairing for conventional polyelectrolyte coacervation that exhibits a salt-suppressed phase behavior. Furthermore, we have found that by tuning the zwitterionic sequence of PA_xM_y polyampholytes with resulting net charge from being negatively charged to positively charged, the coacervate phase of PA_xM_y-$\{W_{12}\}$ complexes can be also broadened. We deduce that excess negatively charged AMPS monomers could weaken the binding between PA_xM_y and $\{W_{12}\}$, while excess positively charged MAPTAC monomers could conversely enhance the binding. Future experimental and theoretical investigation on it would be highly desired. More importantly, linear and non-linear rheological results have shown that both the strength of measured shear moduli and γ_c follow the same trend of $PA_{45}M_{55} > PA_{50}M_{50} > PA_{55}M_{45}$, suggesting that the interaction strength between PA_xM_y and $\{W_{12}\}$ decreases with polyampholytes from being net positively charged to net negatively charged. By varying either AMPS or MAPTAC monomer fraction by merely ±5% from the effective net neutral case, the viscoelasticity of PA_xM_y-$\{W_{12}\}$ coacervates can be modified by 4-5 folds. As combined, all the results indicate that the zwitterionic sequence and resulting net charge of polyampholytes could be employed as a simple tuning parameter to fine control the interaction and material properties of biomimetic complex coacervates as new functional materials for emerging applications.

Supporting Information

The Supporting Information is available free of charge on the xxx at DOI:
Additional experimental results and data analysis (PDF)

Acknowledgements

The authors acknowledge the financial support from the National Science Foundation (NSF DMR-1743041) for this work. The authors thank the Lumigen Instrument Center at Wayne State University for the use of X-Ray Fluorescence Spectrometer.

Reference:

1. M. Gradzielski and I. Hoffmann, *Current Opinion in Colloid & Interface Science*, 2018, **35**, 124-141.
2. M. Skepö and P. Linse, *Macromolecules*, 2003, **36**, 508-519.
3. E. Kizilay, A. B. Kayitmazer and P. L. Dubin, *Advances in Colloid and Interface Science*, 2011, **167**, 24-37.
4. I. S. Tavares, A. L. P. F. Caroni, A. A. D. Neto, M. R. Pereira and J. L. C. Fonseca, *Colloids and Surfaces B: Biointerfaces*, 2012, **90**, 254-258.
5. J. v. d. Gucht, E. Spruijt, M. Lemmers and M. A. Cohen Stuart, *Journal of Colloid and Interface Science*, 2011, **361**, 407-422.
6. W. M. Aumiller, F. Pir Cakmak, B. W. Davis and C. D. Keating, *Langmuir*, 2016, **32**, 10042-10053.
7. T. Moschakis and C. G. Biliaderis, *Current Opinion in Colloid & Interface Science*, 2017, **28**, 96-109.
8. L. Jourdain, M. E. Leser, C. Schmitt, M. Michel and E. Dickinson, *Food Hydrocolloids*, 2008, **22**, 647-659.
9. F. Weinbreck, R. de Vries, P. Schrooyen and C. G. de Kruif, *Biomacromolecules*, 2003, **4**, 293-303.
10. T. H. Kalantar, C. J. Tucker, A. S. Zalusky, T. A. Boomgaard, B. E. Wilson, M. Ladika, S. L. Jordan, W. K. Li, X. Zhang and C. G. Goh, *J Cosmet Sci*, 2007, **58**, 375-383.
11. A. Kishimura, A. Koide, K. Osada, Y. Yamasaki and K. Kataoka, *Angewandte Chemie International Edition*, 2007, **46**, 6085-6088.
12. W. C. Blocher and S. L. Perry, *WIREs Nanomedicine and Nanobiotechnology*, 2017, **9**, e1442.
13. D. S. Hwang, H. Zeng, A. Srivastava, D. V. Krogstad, M. Tirrell, J. N. Israelachvili and J. H. Waite, *Soft Matter*, 2010, **6**, 3232-3236.
14. W. Wei, Y. Tan, N. R. Martinez Rodriguez, J. Yu, J. N. Israelachvili and J. H. Waite, *Acta Biomaterialia*, 2014, **10**, 1663-1670.
15. R. J. Stewart, J. C. Weaver, D. E. Morse and J. H. Waite, *Journal of Experimental Biology*, 2004, **207**, 4727.
16. H. G. B. de Jong and H. R. Kruyt, *Kolloid-Zeitschrift*, 1930, **50**, 39-48.
17. E. A. Frankel, P. C. Bevilacqua and C. D. Keating, *Langmuir*, 2016, **32**, 2041-2049.
18. T. Y. D. Tang, M. Antognozzi, J. A. Vicary, A. W. Perriman and S. Mann, *Soft Matter*, 2013, **9**, 7647-7656.
19. J. Fu and J. B. Schlenoff, *Journal of the American Chemical Society*, 2016, **138**, 980-990.
20. Z. Ou and M. Muthukumar, *The Journal of Chemical Physics*, 2006, **124**, 154902.
21. L.-W. Chang, T. K. Lytle, M. Radhakrishna, J. J. Madinya, J. Vélez, C. E. Sing and S. L. Perry, *Nature Communications*, 2017, **8**, 1273.
22. M. Radhakrishna, K. Basu, Y. Liu, R. Shamsi, S. L. Perry and C. E. Sing, *Macromolecules*, 2017, **50**, 3030-3037.
23. E. Spruijt, A. H. Westphal, J. W. Borst, M. A. C. Stuart and J. van der Gucht, *Macromolecules*, 2010, **43**, 6476-6484.
24. J. T. G. Overbeek and M. J. Voorn, *J. Cell. Comp. Physiol.*, 1957, **49**, 7-26.
25. J. Huang, F. J. Morin and J. E. Laaser, *Macromolecules*, 2019, **52**, 4957-4967.
26. Y. Wang, K. Kimura and P. L. Dubin, *Macromolecules*, 2000, **33**, 3324-3331.
27. P. K. Jha, P. S. Desai, J. Li and R. G. Larson, *Polymers*, 2014, **6**, 1414-1436.

28. K. Glinel, A. Moussa, A. M. Jonas and A. Laschewsky, *Langmuir*, 2002, **18**, 1408-1412.
29. Q. Sun, Z. Tong, C. Wang, B. Ren, X. Liu and F. Zeng, *Polymer*, 2005, **46**.
30. H. Dautzenberg and W. Jaeger, *Macromol. Chem. Phys.* , 2002, **2002**, 3270-3275.
31. A. B. Kayitmazer, A. F. Koksal and E. Kilic Iyilik, *Soft Matter*, 2015, **11**, 8605-8612.
32. H. Espinosa-Andrews, K. E. Enríquez-Ramírez, E. García-Márquez, C. Ramírez-Santiago, C. Lobato-Calleros and J. Vernon-Carter, *Carbohydrate Polymers*, 2013, **95**, 161-166.
33. M. Lemmers, J. Sprakel, I. K. Voets, J. van der Gucht and M. A. Cohen Stuart, *Angewandte Chemie International Edition*, 2010, **49**, 708-711.
34. M. Dompé, F. J. Cedano-Serrano, M. Vahdati, U. Sidoli, O. Heckert, A. Synytska, D. Hourdet, C. Creton, J. van der Gucht, T. Kodger and M. Kamperman, *International Journal of Molecular Sciences*, 2020, **21**.
35. P. G. Lawrence and Y. Lapitsky, *Langmuir*, 2015, **31**, 1564-1574.
36. E. Spruijt, M. A. Cohen Stuart and J. van der Gucht, *Macromolecules*, 2013, **46**, 1633-1641.
37. M. Rubinstein and A. N. Semenov, *Macromolecules*, 1998, **31**, 1386-1397.
38. E. Spruijt, J. Sprakel, M. Lemmers, M. A. C. Stuart and J. van der Gucht, *Physical Review Letters*, 2010, **105**, 208301.
39. T. K. Lytle, L.-W. Chang, N. Markiewicz, S. L. Perry and C. E. Sing, *ACS Central Science*, 2019, **5**, 709-718.
40. A. M. Rumyantsev, N. E. Jackson, B. Yu, J. M. Ting, W. Chen, M. V. Tirrell and J. J. de Pablo, *ACS Macro Lett.*, 2019, **8**, 1296-1302.
41. C. E. Sing and S. L. Perry, *Soft Matter*, 2020, **16**, 2885-2914.
42. V. N. Uversky, I. M. Kuznetsova, K. K. Turoverov and B. Zaslavsky, *FEBS Letters*, 2015, **589**, 15-22.
43. Timothy J. Nott, E. Petsalaki, P. Farber, D. Jervis, E. Fussner, A. Plochowietz, T. D. Craggs, David P. Bazett-Jones, T. Pawson, Julie D. Forman-Kay and Andrew J. Baldwin, *Molecular Cell*, 2015, **57**, 936-947.
44. X. Zhang, Y. Lin, N. A. Eschmann, H. Zhou, J. N. Rauch, I. Hernandez, E. Guzman, K. S. Kosik and S. Han, *PLOS Biology*, 2017, **15**, e2002183.
45. J. J. Madinya, L.-W. Chang, S. L. Perry and C. E. Sing, *Molecular Systems Design & Engineering*, 2020, **5**, 632-644.
46. J. McCarty, K. T. Delaney, S. P. O. Danielsen, G. H. Fredrickson and J.-E. Shea, *The Journal of Physical Chemistry Letters*, 2019, **10**, 1644-1652.
47. B. Jing, D. Xu, X. Wang and Y. Zhu, *Macromolecules*, 2018, **51**, 9405-9411.
48. B. Jing, J. Qiu and Y. Zhu, *Soft Matter*, 2017, **13**, 4881-4889.
49. B. Khadro, I. Baroudi, A.-M. Goncalves, B. Berini, B. Pegot, F. Nouar, T. N. Ha Le, F. Ribot, C. Gervais, F. Carn, E. Cadot, C. Mousty, C. Simonnet-Jégat and N. Steunou, *Journal of Materials Chemistry A*, 2014, **2**, 9208-9220.
50. R. Neumann, *Prog. Inorg. Chem.*, 1998, **47**, 317-370.
51. C. L. Hill and C. M. Prosser-McCartha, *Coordination Chemistry Reviews*, 1995, **143**, 407-455.
52. J. Lehmann, A. Gaita-Ariño, E. Coronado and D. Loss, *Nature Nanotechnology*, 2007, **2**, 312-317.
53. J. T. Rhule, C. L. Hill and D. A. Judd, *Chem. Rev.*, 1998, **98**, 327-357.
54. C. L. Hill, M. S. Weeks and R. F. Schinazi, *J. med. chem. (Print)*, 1990, **33**, 2767-2772.

55. A. B. Lowe and C. L. McCormick, *Chem. Rev.*, 2002, **102**, 4177-4190.
56. O. Azzaroni, A. A. Brown and W. T. S. Huck, *Angewandte Chemie International Edition*, 2006, **45**, 1770-1774.
57. P. Mary, D. D. Bendejacq, M.-P. Labeau and P. Dupuis, *The Journal of Physical Chemistry B*, 2007, **111**, 7767-7777.
58. Y.-J. Shih and Y. Chang, *Langmuir*, 2010, **26**, 17286-17294.
59. in *Practical Environmental Analysis*, eds. M. Radojević and V. N. Bashkin, The Royal Society of Chemistry, 1999, pp. 138-273.
60. L. Yoder, *Journal of Industrial & Engineering Chemistry*, 1919, **11**, 755-755.
61. K. G. Kehl and V. R. Meyer, *Anal. Chem.*, 2001, **73**, 131-133.
62. M. Boström, V. S. J. Craig, R. Albion, D. R. M. Williams and B. W. Ninham, *The Journal of Physical Chemistry B*, 2003, **107**, 2875-2878.
63. J. J. Spitzer, *The Journal of Physical Chemistry B*, 2003, **107**, 10319-10319.
64. R. Sjöback, J. Nygren and M. Kubista, *Spectrochimica Acta Part A: Molecular and Biomolecular Spectroscopy*, 1995, **51**, L7-L21.
65. F. Wang, J. Yang and J. Zhao, *Polymer International*, 2015, **64**, 999-1005.
66. H. Charaya, X. Li, N. Jen and H.-J. Chung, *Langmuir*, 2019, **35**, 1526-1533.
67. Q. Shao, Y. He and S. Jiang, *The Journal of Physical Chemistry B*, 2011, **115**, 8358-8363.
68. T. Wang, X. Wang, Y. Long, G. Liu and G. Zhang, *Langmuir*, 2013, **29**, 6588-6596.
69. Q. Wang and J. B. Schlenoff, *Macromolecules*, 2014, **47**, 3108-3116.
70. C. L. McCormick and L. C. Salazar, *Macromolecules*, 1992, **25**, 1896-1900.
71. S. Adhikari, V. M. Prabhu and M. Muthukumar, *Macromolecules*, 2019, **52**, 6998-7004.
72. H. H. Winter and M. Mours, in *Neutron Spin Echo Spectroscopy Viscoelasticity Rheology*, Springer Berlin Heidelberg, Berlin, Heidelberg, 1997, pp. 165-234.
73. H. H. Winter, in *Structure and Dynamics of Polymer and Colloidal Systems*, eds. R. Borsali and R. Pecora, Springer Netherlands, Dordrecht, 2002, pp. 439-470.

Table of Contents Entry

Effect of polyampholyte net charge on the phase diagram and viscoelasticity of polyzwitterion-polyoxometalate coacervates